Int. J. Electrochem. Sci., 17 **(2022)** Article ID: 22091, doi: 10.20964/2022.09.03

International Journal of
ELECTROCHEMICAL
SCIENCE
www.electrochemsci.org

Short Communication

Controllable Leaching of Ag_2WO_4 Template for Production of Ni-Co-P Nanosheets as Electrocatalyst for Hydrogen Evolution

Bao-Yu Guo[1], *Yi-Wei Wang*[2], *Bin Dong*[1,*]

[1] College of Science, China University of Petroleum (East China), Qingdao 266580, PR China
[2] College of Resources and Environment, Southwest University, Chongqing 400715, PR China
[*]E-mail: dongbin@upc.edu.cn

Received: 7 July 2021 / *Accepted:* 22 August 2021 / *Published:* 7 August 2022

The transition metal-based phosphides as earth-abundant electrocatalysts demonstrate the promising activity and stability for efficient hydrogen evolution reaction (HER) in alkaline solution. To further enhance the HER performance of phosphides, hierarchical Ni-Co-P nanosheets (Ni-Co-P NS) have been prepared through a facile etching template (Ag_2WO_4) method and following phosphating process. The disappearance of Ag_2WO_4 can effectively promote the full contact between Ni-Co phosphide and electrolyte. Benefiting from the well dispersion of active nanoparticles, the synergistic effect of Ni_2P and Co_2P and the abundant active sites from Ni-Co-P NS, the optimized binary metal Ni-Co-P NS exhibits excellent HER performance with a low overpotential of 74.6 mV to achieve the current density of 10 mA cm^{-2}, which is similar to that of Pt/C with an overpotential of 54.9 mV at 10 mA cm^{-2}. The stability measurements confirm the excellent stability of Ni-Co-P NS, which may be due to the intimate combination of Ni_2P and Co_2P nanoparticles. The enhanced HER mechanisms have been discussed in detail. This etching-template method may provide a new choice for designing and synthesizing transition metal-based electrocatalysts for water splitting.

Keywords: binary meal phosphides; nanosheet; ethching-template; hydrogen evolution reaction

1. INTRODUCTION

Renewable energy has accumulated much attention due to its environmental friendliness, renewablility and low cost [1-5]. As the renewable energy, hydrogen has been regarded as a new potential energy carrier owing to its cleanliness and high energy density. Electrocatalytic water splitting, as a means of efficient way, provides a low-carbon and environmental friendly process for hydrogen production [6-12]. However, the large overpotential that occur in the cathode reaction process limits the industrial application of water splitting [13-19]. Therefore, searching for high active and efficient catalyst to lower the overpotential is great significance for large-scale hydrogen production. So far, many researches have demonstrated that best catalysts for hydrogen evolution reaction (HER) are precious

metal-based catalysts, such as Pt and Pt-based metal catalysts. However, their high cost and rarity cause a great challenge for their sustainability. So, it is necessary to develop alternative non-precious-based HER electrocatalysts with high activity and reserve [20-23].

The first-row transition metals and their compounds are considered to be the most potential substitutes for precious metals due to their excellent electrochemical properties and abundance in the earth [24-27]. At present, phosphides (Co_2P, Ni_2P) [28-30], selenides (NiSe, $MoSe_2$) [31, 32], nitrides (Ni_2N, Ni_3Mo_3N) [33-35], carbides (Mo_2C) [36, 37], and metal alloys ($MoNi_4$) [38] have been investigated as efficient HER catalysts. Among them, metal phosphides are particularly prominent because the mechanism for hydrogen evolution of them is similar to that of bio-hydrogenase in alkaline environment. For example, Horn's group has found that the pure CoP has a relatively high catalytic activity on HER, where P atom can be used as the true active site [39]. Chen et al. reported that with the addition of nickel, the ternary NiCoP catalyst could possess a more appropriate hydrogen adsorption energy and higher catalytic activity than CoP alone [40]. Simultaneously, Luo et al. further modified it by borrowing the carrier of MOF, and the optimized CoP/Co-MOF hybrids demonstrated Pt-like activity with the onset overpotential of only 34 and 27 mV for HER in alkaline and acidic solution, respectively [41]. However, the above materials mainly focus on the decoration of a single area (catalyst-electrolyte), while the development of the other side is barely mentioned (catalyst-support). Therefore, there is still a large potential to develop the better electrocatalytic performances of them.

Currently, optimizing the morphology and nanostructures of catalysts to fully expose active species are the most common method to improve the electrocatalytic activity for HER [42]. To solve this problem, many kinds of templates and substrates are widely considered such as hollow carbon spheres, carbon nanotubes, silver tungstate nanoblock, graphene nanocrystals, Prussian blue analogues, etc. Among them, the silver tungstate (Ag_2WO_4) with block structure is particularly prominent since it can provide larger area to load more primary catalysts after etched by a certain-concentration acid solution. Where, the Ag_2WO_4 support resolves in the solution and the main catalyst can be fully leaked in the electrolyte, thus promoting the rapid mass transfer process. [43].

Inspired by the above analysis, we design an etching-template method by using Ag_2WO_4 nanocuboid as self-sacrificed precursors and Ni-Co-P NS are synthesized through facile phosphorization process. Firstly, it can be seen in Scheme 1 that the prepared Ag_2WO_4 nanocuboid as template is used to disperse Ni and Co element by constructing uniform Ag_2WO_4-Ni-Co nanocuboid with rough surface. Secondly, the calcined Ag_2WO_4@Ni-Co hybrids has been be etched, then Ni-Co-O nanosheets have been obtained. Thirdly, a facile phosphorization process has been conducted for Ni-Co-O nanosheets to synthesize Ni-Co-P NS. This facile etching-template combined with phosphorization method suggest more exposed active sites for HER and keep the good electronic transfer rate. The electrochemical measurements results clearly show that Ni-Co-P NS has a remarkable activity with a low overpotential of only 74.6 mV to reach the current density of 10 mA cm^{-2} in alkaline solution for HER, which is similar to Pt/C catalyst (54.9 mV at 10 mA cm^{-2}). The enhanced mechanisms have been systematically investigated. The results provide the guidance for exploring binary metal phosphides with unique structures as efficient HER catalysts.

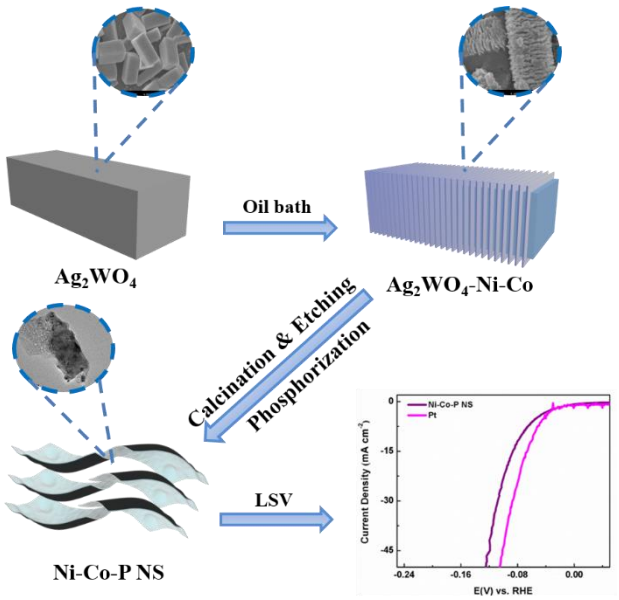

Scheme. 1 The Schematic representation of HER process Ni-Co-P NS.

2. EXPERIMENTAL SECTION

2.1 Ag_2WO_4 synthesis

To prepare Ag_2WO_4 precursor, 1.36 g of $AgNO_3$ and 1.0 g of polyvinyl pyrrolidone (PVP) were added into 40 mL of deionized water (DI) with the help of stirring to acquire solution A. Subsequently, 272 mg of Na_2WO_4 and 1.0 g of polyvinyl pyrrolidone were dispersed in 30 mL of DI to obtain solution B. Then, the solution B was slowly added to the solution A under vigorous stirring with a magnetic stirring for 30 min to get the gray solution. After that, the precursor was placed in a microwave reflux reactor and refluxing it for 20 min at a temperature of 90 ℃. Finally, the obtained sample was collected by the centrifugation and washed with deionized water (DI) and ethanol at least twice and then dried at 60 ℃ for 8 h.

2.2 Ag_2WO_4@Ni-Co synthesis

To obtain Ag_2WO_4@Ni-Co hybrids, 0.2 g of the Ag_2WO_4 precursor, 1.2 g of $Co(NO_3)_2{\cdot}6H_2O$, 0.6 g of $Ni(NO_3)_2{\cdot}6H_2O$, 2.0 g of urea, 2.0 g of polyvinyl pyrrolidone, 140 ml anhydrous ethanol and 20 ml DI were put into a single-mouthed circular bottom flask, and then were stirred for 5 h in an oil bath. After cooling down to ambient temperature, the resulted suspension was treated by centrifugation, washed with DI water and absolute ethanol for two times, and finally dried at 60 ℃ for 8 h.

2.3 Ni-Co-O synthesis

For synthesis of the Ni-Co-O nanosheets, 0.04 g of the Ag_2WO_4@Ni-Co hybrids were put into a porcelain boat and then annealed at 300 ℃ in muffle furnace for 2 h with a heating rate of 2 ℃ min^{-1}. After that, the obtain sample was dissolved into 40 mL DI containing 20 mL 1.0 M HNO_3 solution and 20 mL 1.0 M $NH_3{\cdot}H_2O$ for stirring. The role of HNO_3 here is used to accelerate the dissolution of

Ag_2WO_4 precursor. $NH_3•H_2O$ can coordinate well with the Ag^+ to promote the formation of $[Ag(NH_3)_2]^+$ solution. So the etching process can be realized. After 20 min reaction, the Ag_2WO_4 can be etched away. And the obtained nanosheets were washed with the same method for two times, and finally dried at 60 ℃ overnight.

2.4 Ni-Co-P NS synthesis

For preparation of Ni-Co-P NS, 0.04 g of Ni-Co-O and 0.8 g of NaH_2PO_2 were put into a magnetic boats. Subsequently, the porcelain boat containing the sample was placed in a tube furnace for phosphorization at a temperature of 300 ℃ for two hours with a heating rate of 2 ℃ min^{-1} in argon. After cooling down to room temperature, the black Ni-Co-P NS was prepared.

2.5 Ni-Co-P NC synthesis

The method of synthesizing the Ni-Co-P NC is in the same way as Ni-Co-P NS excepting that Ag_2WO_4 nanocuboid was not added as support.

2.4 Material characterization

X-ray diffraction (XRD) of all samples was examined on a X'Pert PRO MPD system with the scanning rate was 10° min^{-1} and equipped with a Cu Kα radiation source. The crystal structure and element distribution of sample were research by TEM and HRTEM images on a FEI Tecnai G^2 at 200 kV. X-ray photoelectron spectroscopy (XPS) was measured on a Perkin-Elmer model PHI 5600 XPS system with Al Kα radiation (hυ = 1486.6 eV) as a monochromatic X-ray source for excitation to determine the structure of the compound. SEM images were obtained on a Hitachi, S-4800 with the 15 kV accelerating voltage to analysis hybrid morphology.

2.5 Electrochemical tests

Electrochemical tests for all catalyst were conducted in 1.0 M KOH in a three-electrode system that using Gamry Reference 600 Instruments electrochemistry workstation at room temperature. A glassy carbon electrode with a different precursor, a saturated calomel electrode (saturated KCl solution) and a graphite rod were used as the working electrode, the reference electrode and the counter electrode, respectively. Linear sweep voltammetry (LSV) measurements were conducted at a scan rate of 2 mV s^{-1}. And the electrochemical impedance spectroscopy (EIS) measurements were carried out at the potential of -1.16 V vs SCE.

3. RESULTS AND DISCUSSION

Fig.1a shows the XRD data of Ag_2WO_4@Ni-Co, Ag_2WO_4@Ni-Co-O, Ni-Co-O, Ni-Co-P NS and Ag_2WO_4. It can be clearly seen that Ag_2WO_4 exhibits five diffraction peaks with 2θ values of 31.7°, 34.1°, 35.7°, 45.9° and 61.4°, which are in line with the planes of Ag_2WO_4 (PDF No.00-034-0061).

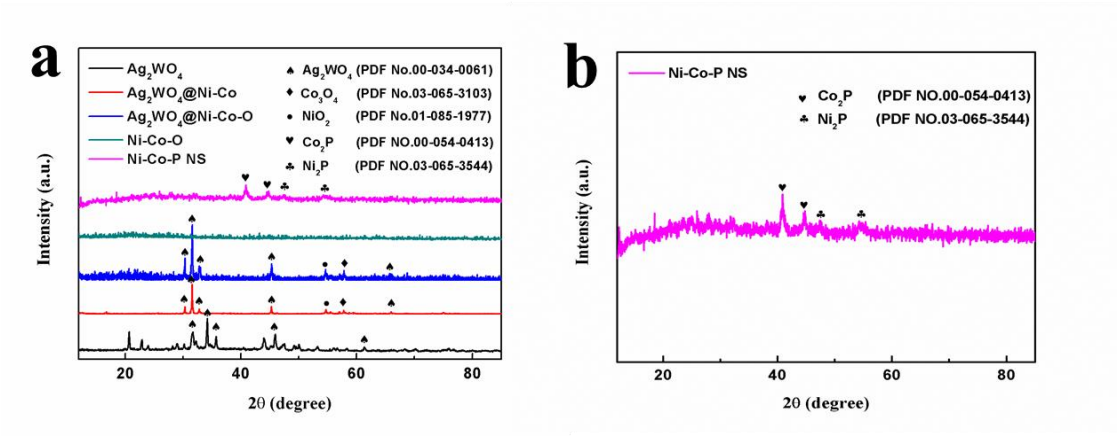

Figure 1. (a) XRD patterns of Ag_2WO_4@Ni-Co, Ag_2WO_4@Ni-Co-O, Ni-Co-O, Ni-Co-P NS and Ag_2WO_4 samples; (b) XRD of Ni-Co-P NS.

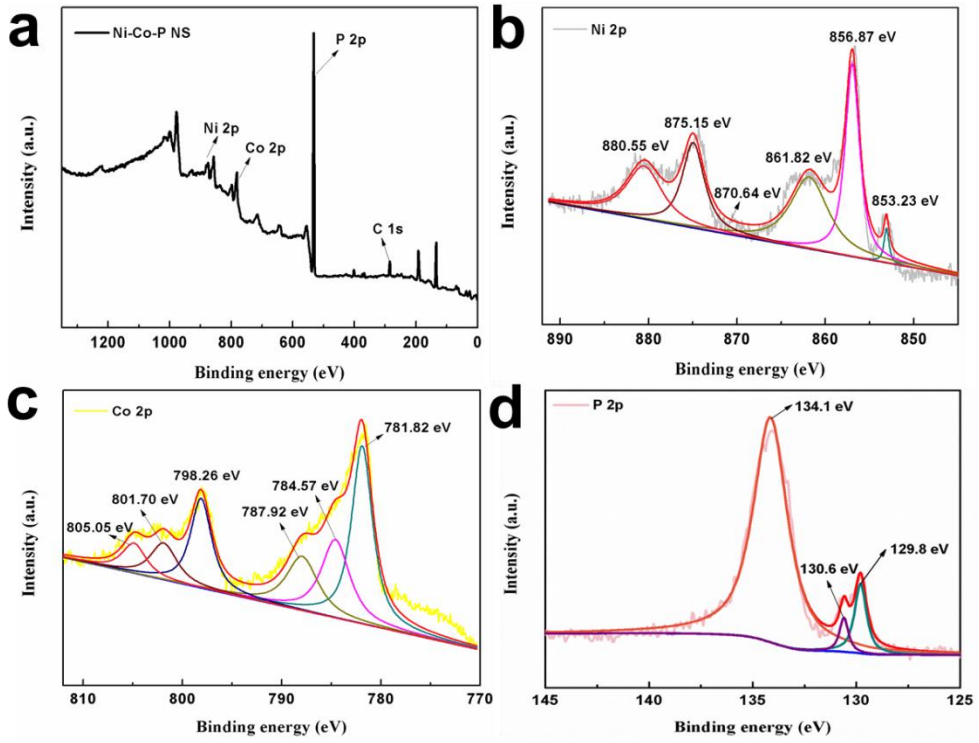

Figure 2. XPS of Ni-Co-P NS sample. (a) Survey; (b) Ni 2p; (c) Co 2p and (d) P 2p.

After the Ni and Co ions are loaded onto the Ag_2WO_4 template with a special chemical reaction, the obtained Ag_2WO_4@Ni-Co shows two peaks at 55.1° and 57.48°, which are in accordance with the crystal facets of NiO_2 (PDF No.01-085-1977) and Co_3O_4 (PDF No.03-065-3103), respectively. When the Ag_2WO_4@Ni-Co is annealed in a muffle furnace, the XRD pattern of Ag_2WO_4@Ni-Co-O has no significant changes. After removing template (Ag_2WO_4) from Ag_2WO_4@Ni-Co-O, it transforms into Ni-Co-O and has no noticeable peak, indicating an amorphous state. Finally, the Ni-Co-P NS is acquired

by a phosphorization method and two obvious peaks at 40.9° and 44.5° are good agreement in the crystal of Ni_2P (PDF NO.03-065-3544) and Co_2P (PDF NO.00-054-0413) (Fig. 1b), respectively.

The elements valence of Ni-Co-P NS has been studied by XPS. The elements including C, Ni, Co and P in Ni-Co-P NS have been confirmed in Fig. 2a. In Fig. 2b, the Ni 2p spectrum demonstrates the two spin-orbit doublet peaks, which may belong to Ni $2p_{1/2}$ and Ni $2p_{3/2}$. The peaks at 856.87 eV and 853.23 eV are originated from Ni^{3+} and Ni^{2+} of Ni $2p_{3/2}$.At the same time, those at 875.15 eV and 870.64 eV may be the signal of Ni^{3+} and Ni^{2+} of Ni $2p_{1/2}$, respectively [44]. The characteristic peaks at the binding energies of 861.82 eV and 880.55 eV are satellite peaks (Sat.). As shown in Fig. 2c, the peaks at 801.70 and 798.26 eV may be assigned to Co^{3+} and Co^{2+} of Co $2p_{1/2}$, respectively, and the peaks at 784.57 eV and 781.82 eV belong to that of Co^{3+} and Co^{2+} of Co $2p_{3/2}$. The obvious peaks of Co^{3+} and Co^{2+} with a binding energy of 805.05 eV and 787.92 eV may be ascribed to the satellite peak (Sat.) [41]. For the P 2p spectrum, it may be divided into $2p_{3/2}$ and $2p_{1/2}$ that shown at 130.6 eV and 129.8 eV, which is derived from metal phosphides. Also there are a peak at 134.1 eV, demonstrating the existence of P-O resulting from PO_4^{3-} [29].

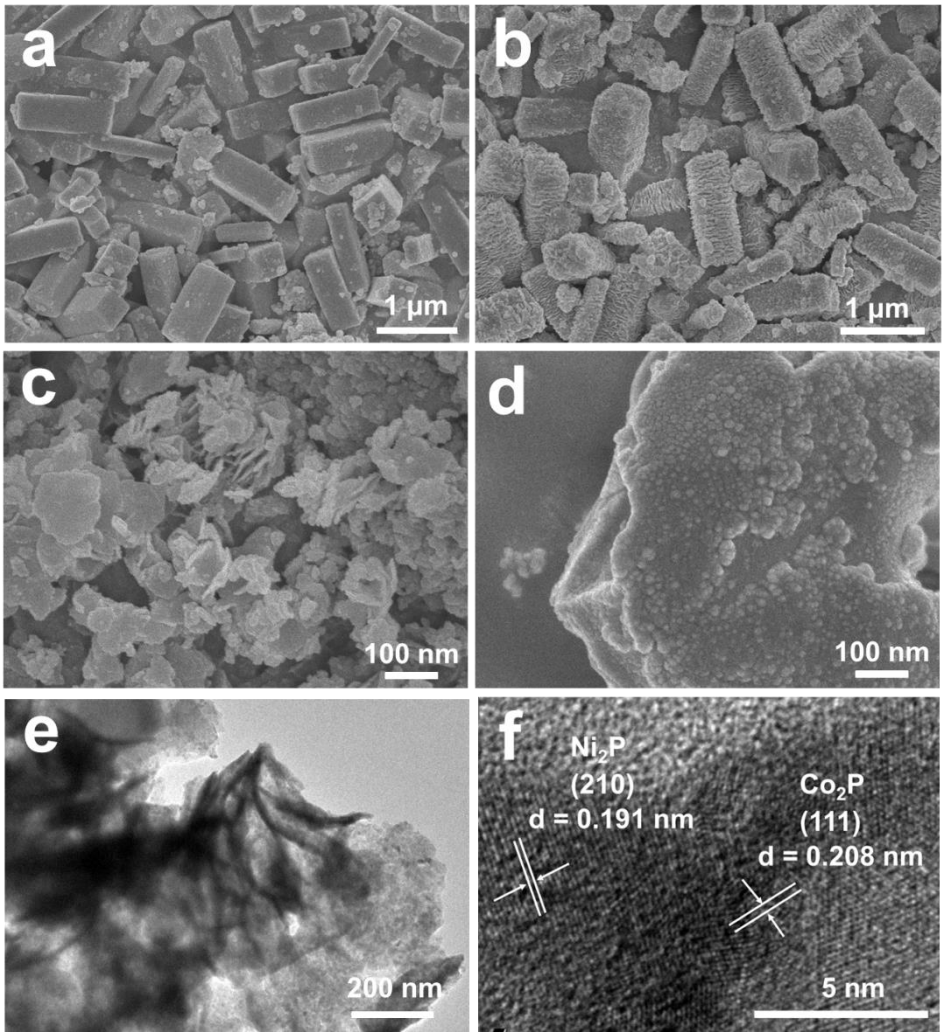

Figure 3. (a) SEM of Ag_2WO_4; (b) SEM of Ag_2WO_4@Ni-Co; (c) SEM of Ni-Co-O; (d) SEM of Ni-Co-P NS and (e, f) HRTEM images of Ni-Co-P NS.

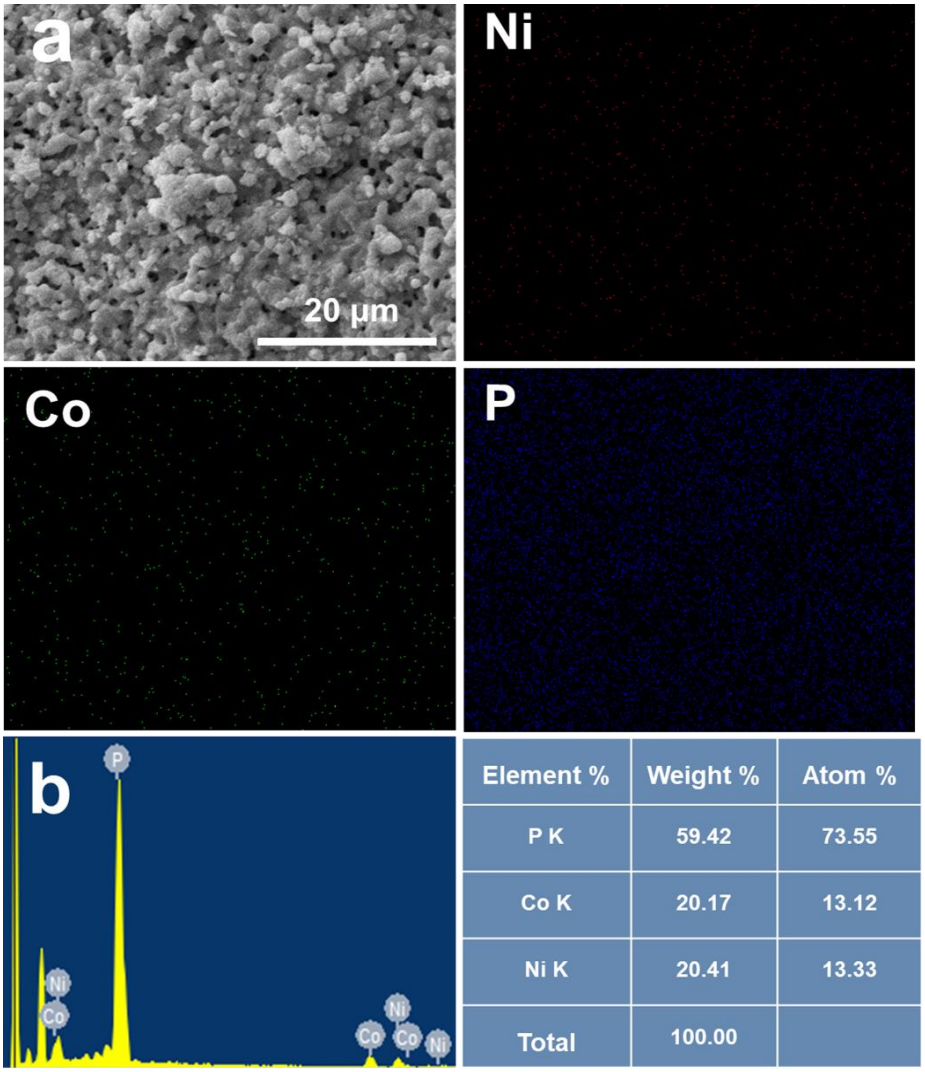

Figure 4. (a) SEM mapping of Ni-Co-P NS and (b) EDX of Ni-Co-P NS.

To furtherly study the microstructure and structure of the precursor Ag_2WO_4, Ag_2WO_4@Ni-Co, Ni-Co-O and Ni-Co-P NS, SEM, HRTEM and SEM mapping are tested in Fig.3 and Fig.4. As shown in Fig. 3a, the Ag_2WO_4 precursor exhibits the cuboid structure with smooth surface, which may provide a large number of active sites. For Ag_2WO_4@Ni-Co, Fig. 3b demonstrates the Ni-Co composite is growing vertically on the surface of Ag_2WO_4, providing a basis for the formation of Ni-Co-P nanosheets. After calcination and nitric acid etching, Ag_2WO_4 has disappeared from the center of the cube and Ag_2WO_4@Ni-Co has transformed into the Ni-Co-O (Fig. 3c), which effectively promote the full contact between the electrolyte and the sample electrocatalyst, thus speeding up the gas transfer process. SEM image of Ni-Co-P NS in Fig. 3d shows that the Ni-Co phosphide nanosheet obtained through a high temperature phosphorization process, where the rougher surface may indicate a higher catalytic activity. Fig. 3e-h show the TEM images of Ni-Co-P NS. The length of the Ni-Co-P nanosheet is approximately to be 300 nm with width estimating at 150 nm. The high-resolution image in Fig. 3d show the lattice fringes with the interplanar spacing of 0.191 and 0.298 nm, corresponding to (210) and (111) planes of

Ni_2P and Co_2P, respectively. Moreover, energy dispersive X-ray (EDX) and SEM mapping (Fig. 4) are employed to analyze the element content and distribution. The above results verify that the elemental molar fraction of Ni and Co in Ni-Co-P NS are 20.17 % and 20.41 %, close to 1:1 atomic ratio.

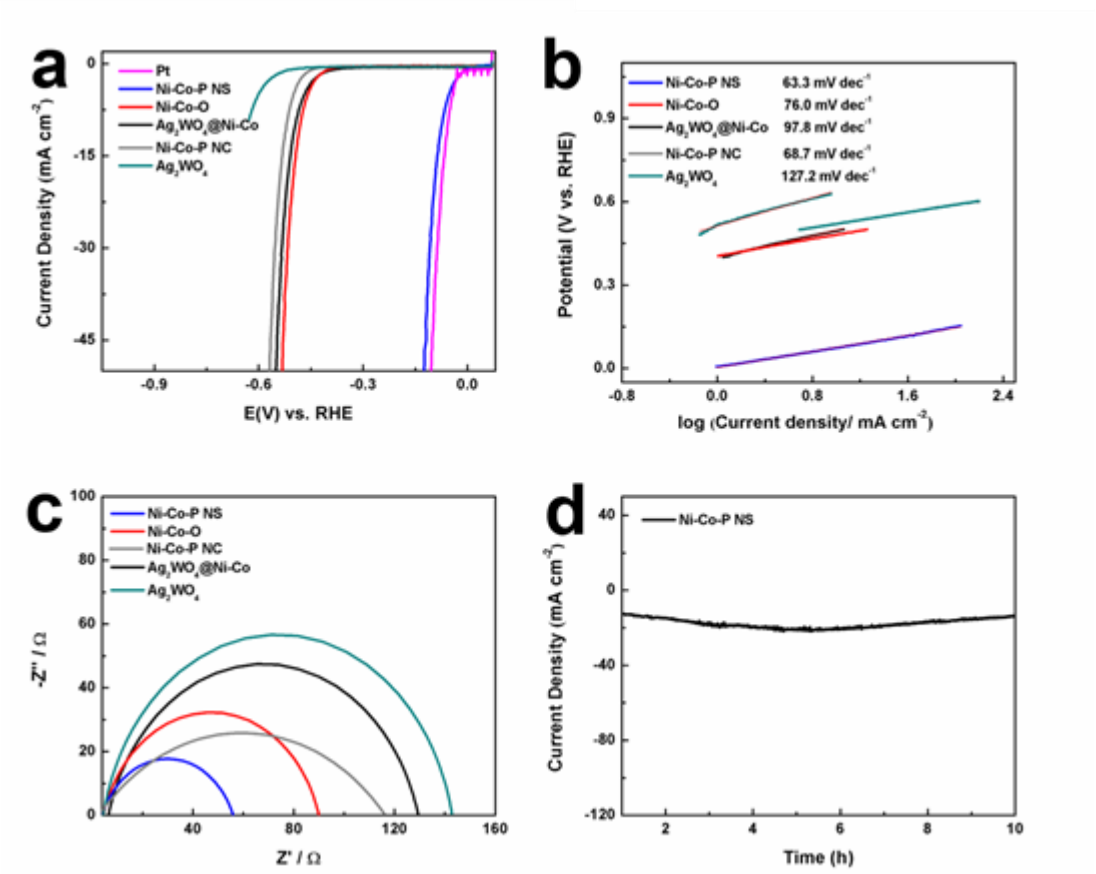

Figure 5. (a) LSV curves of all samples after HER process in1 M KOH, (b) Tafel plots of Ni-Co-P NC, Ag_2WO_4@Ni-Co , Ni-Co-O and Ni-Co-P NS, (c) Electrochemical impedance spectroscopy (EIS) results (d) stability data of Ni-Co-P NS (I-T for 10 h).

The electrochemical HER performances of the catalysts are estimated in Fig. 5. Obviously, the pure Ag_2WO_4 shows the poor activity for HER due to its electrocatalytic inertness. At the current density of 10 mA cm^{-2}, the excellent overpotential of 54.9 mV (vs RHE) of Pt/C has been obtained. Fig. 5a shows that overpotentials of Ni-Co-P NC, Ag_2WO_4@Ni-Co and Ni-Co-O are 561 mV, 547 mV and 528 mV at 10 mA cm^{-2}, respectively. But for Ni-Co-P NS, it possesses a better catalytic property than Ni-Co-P NC. The overpotential of Ni-Co-P NS is much lower and only need 74.6 mV to reach 10 mA cm^{-2}. The comparison of overpotential with other similar literatures has been listed in Table 1. Fig. 5b presents the Tafel slopes of all samples. Ni-Co-P NS shows a smaller Tafel slope of 63.3 mV·dec^{-1} than Ni-Co-P NC (79.3 mV·dec^{-1}), Ag_2WO_4@Ni-Co (97.8 mV·dec^{-1}) and Ni-Co-O (76.0 mV·dec^{-1}), which means a Volmer-Heyrovsky mechanism for Ni-Co-P NS. In Fig. 5c, the Ni-Co-P NS has a smallest diameters means that it possesses the best electro-conductibility, which is favorable for electrochemical activity. At the same time, the stability of Ni-Co-P NS has been investigated by a chronoamperometry

(Fig. 5d). The slight decrease in current density in the long-term reaction indicates a great stability of Ni-Co-P NS in an alkaline solution, which implies the excellent structural stability of Ni-Co-P active sites.

Table 1. Comparison of HER activity between Ni-Co-P NS and other non-precious metal catalyst.

Electrocatalyst	Electrolyte	Overpotential at 10 mA cm^{-2} (mV)	Reference
Ni-Co-P NS	**1 M KOH**	**74.6**	**This work**
PSS-PPy/Ni-Co-P	1 M KOH	67	45
NCS/NCP	1 M KOH	100	46
Ni–Co–P/NF	1 M KOH	156	47
$Ni_{1.5}Co_{1.5}P$/MFs	1 M KOH	141	48
NiCoP/NPC	1 M KOH	80	49
S-NiCoP	1 M KOH	~120	50
P-$Ti_3C_2T_x$@NiCoP	1 M KOH	101	51
NiCoP/NF	1 M KOH	78	52
NiCoP-NPs@GA	1 M KOH	109	53
$NiCo_2S_4$@NiCoP	1 M KOH	108	54

4. CONLUSIONS

In this work, a facile way has been applied to prepare Ni-Co-P NS, which combines the etching template and phosphating methods. The prepared Ni-Co-P NS exhibits more efficient electrochemical hydrogen evolution properties in alkaline conditions than pure Ni-Co-P NC. The excellent HER

performances of Ni-Co-P NS may be owing to that the ultra-thin nanometer sheet etching with a certain concentration of nitric acid can provide more active sites for HER and the good synergistic effect between Ni_2P and Co_2P. This work illustrates that the bimetallic phosphides by etching templates may be a good strategy for improving HER performances.

ACKNOWLEDGEMENTS
This work is financially supported by Qingdao Science and Technology Benefiting People Special Project (20-3-4-8-nsh).

References

1. Y. Huang, Y. Wang, C. Tang, J. Wang, Q. Zhang, Y. Wang and J. Zhang, *Adv. Mater.,* 31 (2019) 1803800.
2. J. F. Qin, M. Yang, T. S. Chen, B. Dong, S. Hou, X. Ma, Y. N. Zhou, X. L. Yang, J. Nan and Y. M. Chai, *Inter. J. Hydrogen Energy,* 45 (2020) 2745.
3. J. Yuan, X. Cheng, H. Wang, C. Lei, S. Pardiwala, B. Yang, Z. Li, Q. Zhang, L. Lei, S. Wang and Y. Hou, *Nano-Micro Lett*., 12 (2020) 104.
4. H. Yang, Y. Wu, G. Li, Q. Lin, Q. Hu, Q. Zhang, J. Liu and C. He， *J. Am. Chem. Soc.,* 141 (2019) 12717.
5. H. Chen, X. Ai, W. Liu, Z. Xie, W. Feng, W. Chen and X. Zou, *Angew. Chem. Int. Ed.,* 58 (2019) 11409.
6. A. Li, H. Ooka, N. Bonnet, T. Hayashi, Y. Sun, Q. Jiang, C. Li and H. Han, R. Nakamura, *Angew. Chem. Int. Ed.,* 58 (2019) 5054.
7. Y. M. Du, M. J. Zhang, Z. C. Wang, Y. R. Liu, Y. J. Liu, Y. L. Geng and L. Wang, *J. Mater. Chem. A,* 7 (2019) 8602.
8. Y. Zhao, X. Zhang, X. Jia, G. I. N. Waterhouse, R. Shi, X. Zhang, F. Zhan, Y. Tao, L.Z. Wu and C. H. Tung, D. O'Hare, T. Zhang, *Adv. Energy Mater.,* 8 (2018) 1703585.
9. Y. M. Chai, X. Y. Zhang, J. H. Lin, J. F. Qin, Z. Z. Liu, J. Y. Xie, B. Y. Guo, Z. Yang and B. Dong, *Inter. J. Hydrogen Energy,* 44 (2019) 10156.
10. Z. Pu, I. S. Amiinu, R. Cheng, P. Wang, C. Zhang, S. Mu, W. Zhao, F. Su, G. Zhang, S. Liao and S. Sun, *Nano-Micro Lett.,* 12 (2020) 21.
11. D. Yan, C. L. Dong, Y. C. Huang, Y. Zou, C. Xie, Y. Wang, Y. Zhang, D. Liu, S. Shen and S. Wang, *J. Mater. Chem. A,* 6 (2018) 805.
12. J. Lai, B. Huang, Y. Chao, X. Chen and S. Guo, *Adv. Mater.,* 31 (2019) 1805541.
13. J.Y. Xie, R.Y. Fan, J.Y. Fu, Y.N. Zhen, M.X. Li, H.J. Liu, Y. Ma, F.L. Wang, Y.M. Chai and B. Dong, *Inter. J. Hydrogen Energy*, 46 (2021) 19962-19970.
14. X. Y. Zhang, B. Y. Guo, Q. W. Chen, B. Dong, J. Q. Zhang, J. F. Qin, J. Y. Xie, M. Yang, L. Wang, Y. M. Chai and C. G. Liu, *Inter. J. Hydrogen Energy,* 44 (2019) 14908.
15. A. Saad, H. Shen, Z. Cheng, R. Arbi, B. Guo, L.S. Hui, K. Liang, S. Liu, J. P. Attfield, A. Turak, J. Wang and M. Yang, *Nano-Micro Lett.*, 12 (2020) 79.
16. X. Y. Yu, X. W. Lou, *Adv. Energy Mater.,* 8 (2018) 1701592.
17. H. Liu, D. Zhao, P. Hu, Y. Liu, X. Wu and H. Xia, *Chem. Eng. J.,* 373 (2019) 485.
18. Z. Zou, T. Wang, X. Zhao, W. J. Jiang, H. Pan, D. Gao and C. Xu, *ACS Catal.,* 9 (2019) 7356.
19. B.Y. Guo, X.Y. Zhang, X. Ma, T.S. Chen, M.L. Wen, X.L. Yang, J.F. Qin, Y.M. Chai, J. Nan and B. Dong, *Inter. J. Hydrogen Energy*, 45 (2020) 9575.
20. X.Y. Zhang, Y.R. Zhu, Y. Chen, S.Y. Dou, X.Y. Chen, B. Dong, B.Y. Guo, D.P. Liu, C.G. Liu and Y.M. Chai, *Chem. Eng. J.*, 399 (2020) 125831.
21. D. Zhang, H. Zhao, B. Huang, B. Li, H. Li, Y. Han, Z. Wang, X. Wu, Y. Pan, Y. Sun, X. Sun, J. Lai

and L. Wang, *ACS Cent. Sci*., 5 (2019) 1991.
22. X. Shang, K.L. Yan, Y. Rao, B. Dong, J.Q. Chi, Y.R. Liu, X. Li, Y.M. Chai and C.G. Liu, *Nanoscale*, 9 (2017) 12353.
23. W.H. Hu, R. Yu, G.Q. Han, Y.R. Liu, B. Dong, Y.M. Chai, Y.Q. Liu and C.G. Liu, *Mater. Lett.*, 161 (2015) 120.
24. W. Zhang, D. Li, L. Zhang, X. She, D. Yang, *J. Energy Chem.,* 39 (2019) 39.
25. B. Dong, J.Y. Xie, N. Wang, W.K. Gao, Y. Ma, T.S. Chen, X.T. Yan, Q.Z. Li, Y.L. Zhou and Y.M. Chai, *Renew. Energy,* 157 (2020) 415.
26. G.Q. Han, Y.R. Liu, W.H. Hu, B. Dong, X. Li, Y.M. Chai, Y.Q. Liu and C.G. Liu, *Mater.Chem. Phy.*, 167 (2015) 271.
27. Y. Hua, Q. Xu, Y. Hu, H. Jiang, C. Li, *J. Energy Chem.,* 37 (2019) 1.
28. S. H. Li, N. Zhang, X. Xie, R. Luque and Y. J. Xu, *Angew. Chem. Int. Ed*., 57 (2018) 13082.
29. S. S. Lu, L. M. Zhang, Y. W. Dong, J. Q. Zhang, X. T. Yan, D. F. Sun, X. Shang, J. Q. Chi, Y. M. Chai and Bin Dong, *J. Mater. Chem*. A, 7 (2019) 16859.
30. J. F. Qin, J. H. Lin, T. S. Chen, D. P. Liu, J. Y. Xie, B. Y. Guo, L. Wang, Y. M. Chai and B. Dong, *J. Energy Chem.,* 39 (2019) 182.
31. H. Wu, X. Lu, G. Zheng and G. W. Ho, *Adv. Energy Mater*., 8 (2018) 1702704.
32. Y. R. Zheng, P. Wu, M. R. Gao, X. L. Zhang, F. Y. Gao, H. X. Ju, R. Wu, Q. Gao, R. You, W. X. Huang, S. J. Liu, S. W. Hu, J. Zhu, Z. Li, S and H. Yu, *Nat. Commun*., 9 (2018) 2533.
33. B. You, X. Liu, G. Hu, S. Gul, J. Yano, D. Jiang and Y. Sun, *J. Am. Chem. Soc.,* 139 (2017) 12283.
34. Y. Li, X. Tan, S. Chen, X. Bo, H. Ren, S. C. Smith and C. Zhao, *Angew. Chem. Int. Ed*., 58 (2019) 461.
35. M. Zhang, Q. Dai, H. Zheng, M. Chen and L. Dai. *Adv. Mater*., 30 (2018) 1705431.
36. C. Lei, W. Zhou, Q. Feng, Y. Lei, Y. Zhang, Y. Chen and J. Qin, *Nano-Micro Lett*., 11 (2019) 45.
37. Q. Hu, X. Liu, B. Zhu, L. Fan, X. Chai, Q. Zhang, J. Liu, C. He and Z. Lin, *Nano Energy*, 50 (2018) 212.
38. J. Zhang, T. Wang, P. Liu, Z. Liao and S. Liu, *Nat. Commun*., 8 (2017) 15437.
39. D. H. Ha, B. H. Han, M. Risch, L. Giordano, K. P. C. Yao, P. Karayaylali and Y. S. Horn, *Nano Energy,* 29 (2016) 37.
40. C. Tang, L. Gan, R. Zhang, W. Lu, X. Jiang, A. M. Asiri, X. Sun, J. Wang and L. Chen, *Nano Lett.*, 15 (2016) 6617.
41. T. Liu, P. Li, N. Yao, G. Cheng, S. Chen, W. Luo and Y. Yin, *Angew. Chem. Int. Ed*., 58 (2019) 4976.
42. Y. Yu, Y. Shi and B. Zhang, *Acc. Chem. Res*., 51 (2018) 1711.
43. C. H. Xiao, B. Zhang and D. Li, *Electrochim Acta.,* 242 (2017) 260.
44. J. Yu, G. Cheng and W. Lu, *J. Mater. Chem*. A, 5 (2017) 11229.
45. F. Tian, S. Geng, L. He, Y. Huang, A. Fauzi, W. Yang, Y. Liu, Y. Yu, Chem. Eng. J., 417 (2021) 129232.
46. X. Zhou, J. Zhou, G. Huang, R. Fan, S. Ju, Z. Mi and M. Shen, *J. Mater. Chem. A*, 6 (2018) 20297.
47. Y. Gong, Z. Xu, H. Pan, Y. Lin, Z. Yang and J. Wang, *J. Mater. Chem. A*, 6 (2018) 12506.
48. T. Chen, M. Qian, X. Tong, W. Liao, Y. Fu, H. Dai and Q. Yang, *Int. J. Hydrogen Energy*, 46 (2021) 29889.
49. Z.B. Li, J. Wang, X.J. Liu, R. Li, H. Wang, Y. Wu, X.Z. Wang and Z.P. Lu, *Scrip. Mater.*, 173 (2019) 51.
50. Y. Qi, L. Zhang, L. Sun, G. Chen, Q. Luo, H. Xin, J. Peng, Y. Li, F. Ma, *Nanoscale*, 12 (2020) 1985.
51. S.M. Kang, M. Kim, J.B. Lee, S. Xu, N.C.S. Selvam, P.J. Yoo, *Nanoscale*, 13 (2021) 12854.
52. D. Wang, Y. Zhang, T. Fei, C. Mao, Y. Song, Y. Zhou, G. Dong, *ChemElectroChem*, 8 (2021) 3064.
53. W. Wei, H. Li, W. Sun, J. Wang, X. Fan, G. Jiang, Z. Jiang and J. Xie, *J. Mater. Sci. Mater. Electron.*, 31 (2020) 13521.

54. H. Su, X. Du and X. Zhang, *Int. J. Hydrogen Energy*, 44 (2019) 30910.